INSTITUTE OF PHYSICS PUBLISHING JOURNAL OF PHYSICS A: MATHEMATICAL AND GENERAL

J. Phys. A: Math. Gen. **36** (2003) 6207–6214 PII: S0305-4470(03)54861-2

Gravitoelectrodynamics in Saturn's F ring: encounters with Prometheus and Pandora

Lorin Swint Matthews and Truell W Hyde

Center for Astrophysics, Space Physics, and Engineering Research, Baylor University, PO Box 97310, Waco, TX 76798-7310, USA

Received 15 October 2002, in final form 2 January 2003
Published 22 May 2003
Online at stacks.iop.org/JPhysA/36/6207

Abstract

The dynamics of Saturn's F ring have been a matter of curiosity ever since Voyagers 1 and 2 sent back pictures of the ring's unusual features. Some of these images showed three distinct ringlets with the outer two displaying a kinked and braided appearance. Many models have been proposed to explain the braiding seen in these images; most of these invoke perturbations caused by the shepherding moons or kilometre-sized moonlets embedded in the ring and are purely gravitational in nature. These models also assume that the plasma densities and charges on the grains are small enough that electromagnetic forces can be ignored. However, Saturn's magnetic field exerts a significant perturbative force on even weakly charged micron- and submicron-sized grains causing the grains to travel in epicyclic orbits about a guiding centre. This study examines the effect of Saturn's magnetic field on the dynamics of micron-sized grains along with gravitational interactions between the F ring's shepherding moons, Prometheus and Pandora. Due to the differences in charge-to-mass ratios of the various sized grains, a phase difference between different size populations is observed in the wavy orbits imposed by passage of the shepherding moons.

PACS numbers: 52.27.Lw, 96.30.Mh, 96.30.Wr

1. Background

Saturn's F ring is one of the most dynamic rings observed in the solar system. While Voyager 1 images showed three distinct ringlets with the outer two displaying a kinked and braided appearance [1], Voyager 2 images showed a much more regular structure with four separate, non-intersecting strands [2]. Both Voyagers 1 and 2 detected brighter clumps within the rings with a temporal dependence ranging from days to months [3].

Photometric data collected by Voyagers 1 and 2 suggested that the general structure of the F ring consisted of a core of centimetre- to millimetre-sized particles ∼1 km in width,

with an envelope of micron- and submicron-sized grains extending ∼50 km inwards [4]. Data collected from the Hubble space telescope in 1995 showed similar features, but resulting fits to the data indicated that the minimum grain size is likely to fall within the range of 0.5 to 1 μm, with a maximum of 28% of the ring material being submicron in size [5].

The F ring lies within the inner part of Saturn's magnetosphere, which contains plasma that rigidly corotates with the planet [6]. Thus the dust in Saturn's F ring can become charged. Since the plasma parameters in the vicinity of the F ring are poorly constrained, the magnitude of the charge on the dust grains is not well known. Estimations of the grain charge for micron and submicron grains within the F ring have ranged from less than one electron [4] to −38 V [7]. The grain charge is of interest since charged grains' orbits will be perturbed by the planetary magnetic field with the magnitude of this perturbation depending primarily on the grain's charge-to-mass ratio. Recently, it has been shown that significant perturbations are possible for even weakly charged grains. This allowed the observed physical characteristics of the F ring, such as the 50 km width of the F ring envelope, to be used to determine that the micron and submicron grains within the envelope are likely weakly negatively charged, with a maximum $|q/m| = 0.03$ C kg^{-1} [8].

The purpose of this study is to examine the interaction of such weakly charged individual grains with the F ring's shepherding moons, Prometheus and Pandora, and compare their orbits to that of the uncharged grains. Complications not addressed in this study are the inclination of the F ring and satellite orbits, collisional damping between ring particles, collective effects of the charged grains and plasma, and the effect of moonlets embedded within the ring.

2. The box_tree algorithm

The numerical code employed in this study is a modified version of box_tree, a self-consistent N-body code developed to study Saturn's rings, planetesimal dynamics and fractal aggregation [9–11]. The current version has been modified to consider charged grains and the electrostatic and magnetic forces acting on them as well as external gravitational potentials such as those produced by shepherding satellites [12]. The code has already been used to model a variety of astrophysical and laboratory dusty plasma environments, including formation of, and wave dispersion, in dust crystals [13, 14], chondrule formation [15] and coagulation in protoplanetary discs [12].

The box code [16] divides the ring into self-similar patches or boxes orbiting the planet where the box size is much greater than the mean radial excursions of the constituent particles. This allows the boxes to be dynamically independent with more distant regions of the ring represented by copies of the simulated region. In a rotating system, particle motions are referenced to the centre of a box that orbits the planet at the local Keplerian velocity. This allows an accurate simulation of the complete ring to be represented by a small number of particles. For example, a simulation utilizing a single box containing 5000 particles is equivalent to simulating a complete ring containing 10^6–10^7 particles. The box code, in providing the external potentials acting on the grains, specifies a coordinate system, the linearized equations of motion and a prescription for handling boundary conditions. The tree code [17] provides a mechanism for the rapid calculation of the interparticle forces by means of a multipole expansion, reducing the CPU scaling time from $O(N^2)$ to $O(N \log N)$ for sufficiently large N. The interparticle forces can then be included as a perturbation to the equations of motion.

2.1. Linearized equations of motion

The acceleration of a charged grain in a planetary magnetic field, **B**, and gravitational field is given by

$$\ddot{\mathbf{R}} = \frac{q}{m}(\mathbf{E} + \dot{\mathbf{R}} \times \mathbf{B}) - \frac{GM_{\mathrm{p}}}{R^3}\mathbf{R} - \nabla\phi \tag{1}$$

where M_{p} is the mass of the planet, **R** is the distance from the centre of the planet to the grain and q and m are the grain's charge in coulombs and mass in kilograms, respectively. The grain–grain gravitational and electrostatic interactions are included in the $-\nabla\phi$ term. The electric field results from the relative motion of the ring particles with respect to the corotating magnetic field and is given by

$$\mathbf{E} = -(\mathbf{\Omega}_{\mathrm{p}} \times \mathbf{R}) \times \mathbf{B}(\mathbf{R}) \tag{2}$$

where $\mathbf{\Omega}_{\mathrm{p}}$ is the angular velocity of the planet.

The equations of motion can be linearized in the box frame, which is rotating about the planet with constant angular velocity $\mathbf{\Omega}_k = \Omega_k \hat{z}$ with magnitude

$$\Omega_k = \sqrt{\frac{\mathbf{G}M}{R_{\mathrm{b}}^3}}. \tag{3}$$

R_{b} is the distance from the box to the planet centre and M is the mass of the central planet. Using the fact that $R_{\mathrm{b}} \gg r$, the position of the particle within the box, the complete set of linearized equations of motion is given by

$$\begin{aligned} \ddot{x} &= F_x + 3\Omega_k^2 x + 2\Omega_k \dot{y} + \ddot{x}_m \\ \ddot{y} &= F_y - 2\Omega_k \dot{x} + \ddot{y}_m \\ \ddot{z} &= F_z - \Omega_k^2 z + \ddot{z}_m \end{aligned} \tag{4}$$

where $\mathbf{F} = -\nabla\phi$ is the sum of the gravitational and electrostatic forces per unit mass due to all other particles and the accelerations due to the magnetic field in each dimension are given by

$$\begin{aligned} \ddot{x}_m &= \frac{q}{m}[(\Omega_k - \Omega_{\mathrm{p}})R_x B_z + \dot{y}B_z - \dot{z}B_y] \\ \ddot{y}_m &= \frac{q}{m}[\dot{z}B_x - \dot{x}B_z] \\ \ddot{z}_m &= \frac{q}{m}[-(\Omega_k - \Omega_{\mathrm{p}})R_x B_x + \dot{x}B_y - \dot{y}B_x]. \end{aligned} \tag{5}$$

2.2. Shepherding satellites and eccentric orbits

The orbits of the F ring, Prometheus and Pandora all have small eccentricities [5, 18]. While the orbits of the shepherding moons can be modelled accurately by box_tree as external gravitational potentials, the box containing the ring particles is at a fixed radial distance and thus models a circular orbit. To include the effect of the F ring's eccentricity, the procedure of Showalter and Burns [19] is followed and the combined eccentricity of the rings and satellite is mapped back to the satellite alone. An 'eccentric displacement vector' **E** is defined with polar coordinates (ae, ω) where a is the maximum radial displacement out of round for a given body, e is the eccentricity and ω is the longitude of the pericentre. Any ring/satellite configuration can thus be described by $a_0, a_1, \mathbf{E}_0$ and $\mathbf{E}_1$, where the subscripts '0' and '1' refer to the ring and satellite, respectively. The effect of the satellite on the ring depends on

$\mathbf{E}_1 - \mathbf{E}_0$. By choosing to set $\mathbf{E}'_0 = 0$ and $\mathbf{E}'_1 = \mathbf{E}_1 - \mathbf{E}_0$, all of the eccentricity can be assigned to the satellite. The effect of the 'primed' satellite on a circular ring is essentially the same as that of the unprimed scenario, in which both the satellite and the ring have eccentric orbits. The reference longitude for the satellite's eccentricity is set at run time, so that the position of the satellite can be varied from closest approach to furthest approach as it passes the centre of the box.

2.3. Boundary conditions

The box_tree code makes use of periodic boundary conditions. In the general case, ghost boxes surround the central box and particles that are near a boundary interact with ghost particles in the neighbouring box. As a particle leaves the central box, it is replaced by its ghost particle entering from the opposite side, keeping the total number of particles in the simulation constant. These boundary conditions were modified slightly to take advantage of special properties of the F ring. Since the F ring is a very narrow ring, the box size is chosen to be much greater than the radial width and vertical thickness of the ring. The maximum box size is determined by the requirement that the magnitude of the Lorentz force due to the planetary magnetic field be greater than the first term neglected in the linearization of the equations of motion. The particles are only able to leave the box in the azimuthal direction, requiring only two ghost boxes. Because the box is a non-inertial, rotating frame, particles that are displaced inwards towards Saturn ($-x$ direction) have a positive azimuthal drift (in the $+y$ direction) while particles displaced outwards ($+x$ direction) have a negative azimuthal drift.

The shepherding satellites have different mean motions about the planet than does the box. Particles that are displaced inwards (travelling faster than the mean motion of the box) will spend more time in the vicinity of Prometheus, the inner shepherding satellite. Likewise slower particles will spend more time in the vicinity of Pandora, the outer satellite. This effect was modelled by tracking the number of azimuthal boundary crossings, n, for each particle. The number of boundary crossings times the length of the box, nL, is added to the azimuthal position of the grain, and this adjusted position is used in calculating the grain–satellite separation and the gravitational force due to the satellite. The grain's unadjusted position within the box is used in calculating the effect of the magnetic field, which is azimuthally symmetric [20].

3. Results

For each run, the orbits of 5000 grains were tracked within a 2800 km box, which corresponds to 0.02 radians of arc at the distance of the F ring. The grain radii followed a power law size distribution with $q = 3.5$ with minimum grain radius $a_{\min} = 0.5\ \mu$m and maximum grain radius $a_{\max} = 10.0\ \mu$m [5]. Grains were initially established within the 50 km F ring envelope without perturbations from shepherding moons. The charged grains follow epicyclic orbits about a guiding centre while uncharged grains have local Keplerian orbits. The plasma parameters in the F ring are not well constrained, with estimates of plasma temperature ranging from $10\ \text{eV} < kT_e < 100\ \text{eV}$ [6] and plasma density ranging from $10\ \text{cm}^{-3} < n_o < 100\ \text{cm}^{-3}$ [21]. For this study, the plasma temperature and density were assumed to be constant across the width of the box. Using the values $kT_e = 20$ eV, $n_o = 100\,\text{cm}^{-3}$ and dust density $N_d = 30\,\text{cm}^{-3}$ [21], calculated grain charges yield $q/m = -0.03\ \text{C kg}^{-1}$ for $a_{\min}$ and $q/m = -3.8 \times 10^{-6}\ \text{C kg}^{-1}$ for $a_{\max}$ [22]. It should be noted that grain charges vary only slightly for $kT_e < 25$ eV and as a result the relative dust to plasma density ratio has relatively small effect on the qualitative results of this study [8].

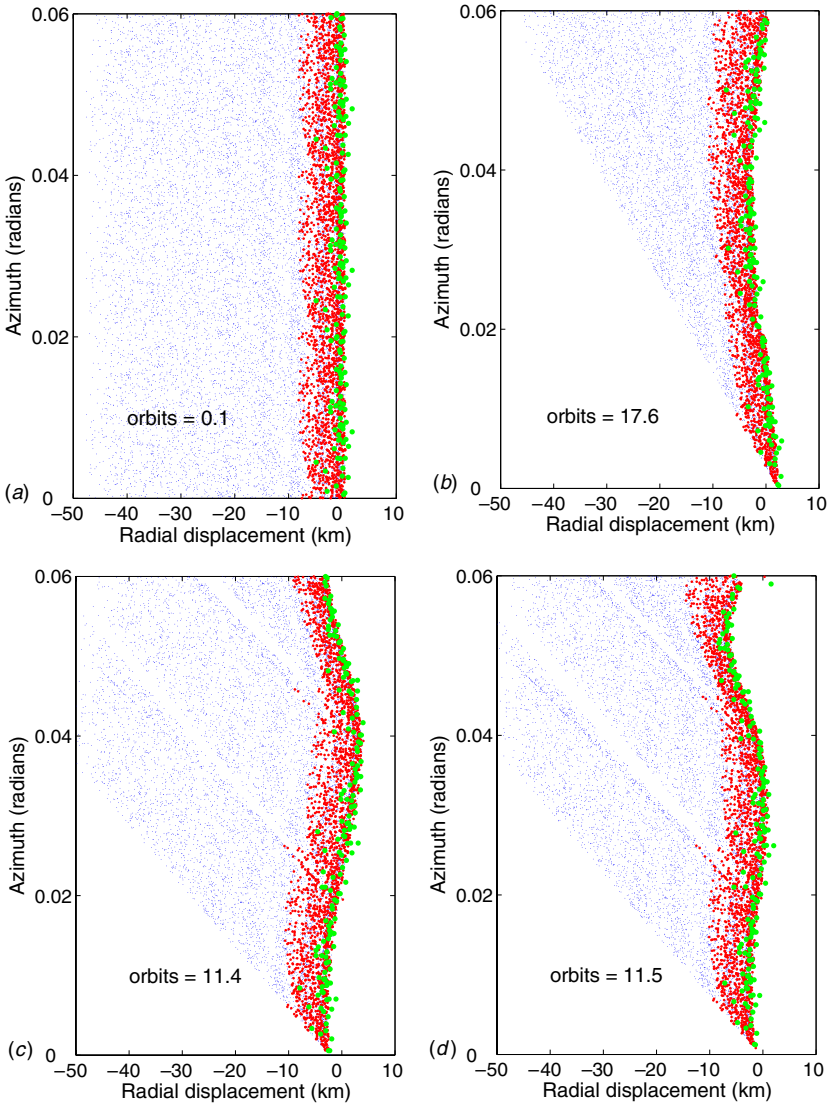

Figure 1. Locations of grains within the F ring after passages of the shepherding satellites. Grains with $r < 1.0$ μm are shown in blue, grains with 1.0 μm $\leqslant a < 3.0$ μm are shown in red, and grains with $r \geqslant 3.0$ μm are shown in green. The initial configuration of the ring particles is shown in (*a*). The smaller charged grains have larger epicyclic orbits due to their higher charge-to-mass ratios. The number of orbits refers to the number of revolutions of the centre of the box about Saturn. (*b*)–(*d*) Uncharged grains after passage of Prometheus, Pandora and both moons simultaneously, respectively. (*e*)–(*g*) Charged grains after passage of Prometheus, Pandora and both moons simultaneously, respectively.

Three types of ring/satellite interactions were modelled: Prometheus alone passing the ring section, Pandora alone passing the ring section and Prometheus and Pandora passing the ring section simultaneously. The simulation was run using three consecutive boxes for each of the three cases with the data for the three concatenated to display a ring section that subtends 0.06 rad. The adjusted azimuthal positions were then plotted for grains that travelled faster than the mean motion of the box.

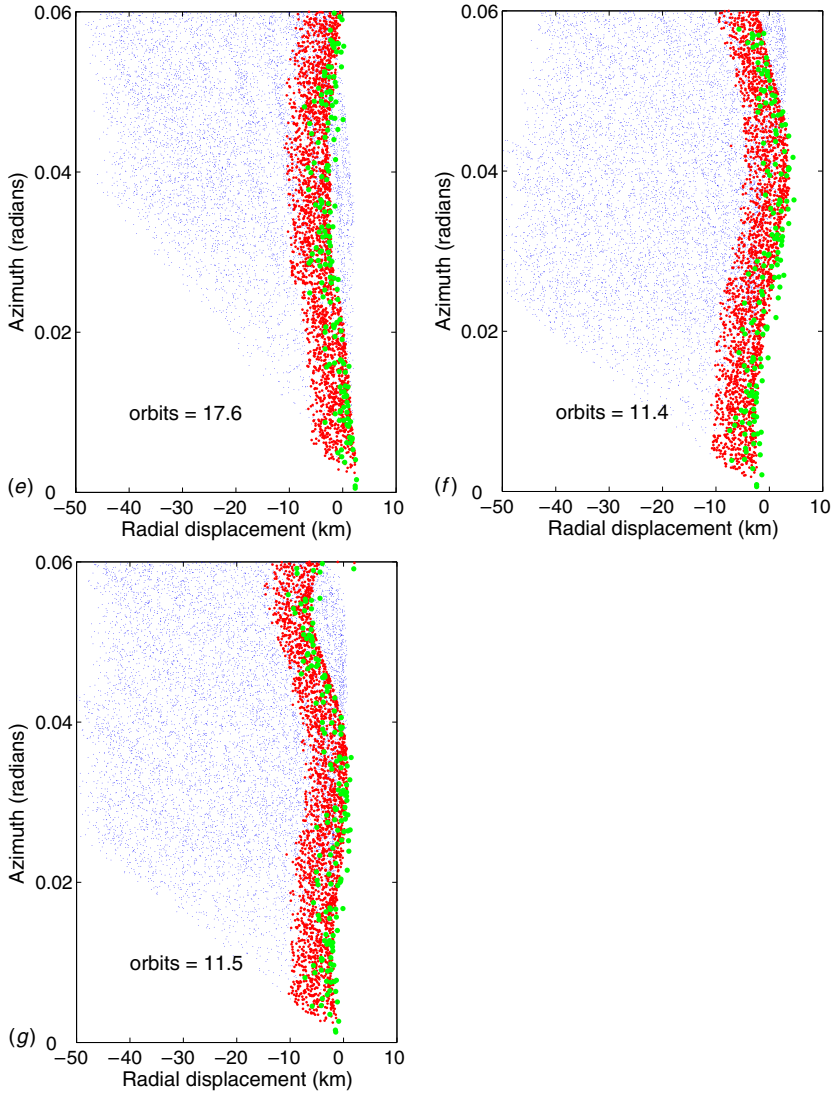

Figure 1. (Continued.)

The initial ring configurations before and after passage of the moon(s) are shown in figure 1 for both charged and uncharged grains. In all three cases with uncharged grains, the passing moon(s) excited a 'rippling' orbit as seen in previous models (e.g. [19]) with the grains, across the entire size range, remaining in phase. However, in the case of weakly charged grains, a distinct phase difference evolves across different size populations with the larger charged grains ($a \geqslant 3.0\ \mu$m) having very similar orbits to the larger uncharged grains. Smaller grains ($a < 1.0\ \mu$m), on epicyclic orbits displaced inwards from the F ring core, have increased orbital velocities and therefore are more strongly affected by Prometheus, the inner moon, and less strongly affected by Pandora, the outer moon. As a result, the orbital behaviour of the charged and uncharged submicron grains differs considerably.

4. Conclusions

This model investigated the effect of Saturn's gravitational and magnetic fields along with the gravitational fields of the shepherding satellites. Appropriate dust number densities were used in calculating the grain charges so that perturbations to individual grain orbits due to their interaction with Saturn's magnetic field could be examined. It has been shown that even very weakly charged grains within Saturn's F ring can have a significant effect on the subsequent orbital behaviour of the ring particles. Even when the grains are not charged strongly enough to display gravitoelectrodynamic resonances with the shepherding moons, the differing charge-to-mass ratios over the various size grains will lead to phase differences in the rippling orbits imposed on the ring particles by the passing moons. This effect may in turn contribute to the observed braiding in the F ring. Although size sorting due to charged grains has been reported previously in planetary magnetospheres [23, 24], such sorting has not been seen for very weakly charged grains (charges as small as one electron). For the dust particle densities utilized in this model, the interparticle forces, which are calculated by the tree part of the code, are insignificant when compared to the planetary gravitational and magnetic forces. The code is currently being modified (parallelized) to facilitate future studies with smaller box sizes, higher dust densities and evolving grain charges, which will allow the effect of collisional damping and the collective effects of charged grains to be determined.

Although the dust density used in this model is still too low to properly assess the collective effects of the charged dust grains with the plasma, it is interesting to note that distinct dusty plasma clouds repel each other due to interaction of the plasma sheaths at the boundaries (Morfill, personal communication 2002). If the phase differences created by the shepherding moons truly separate the dust into different populations according to size, it is possible that these populations would resist recombination, helping to preserve distinct ringlets. The arrival of Cassini at Saturn in 2004 will provide an opportunity to investigate the structure of the F ring and its plasma environment in detail. It would be instructive to learn if separate strands have differing size populations, or if there is a size gradient across the width of the F ring envelope. Such a size sorting would confirm the presence of charged grains within the F ring and underscore the importance of including even very weak charge effects in modelling ring structures.

References

[1] Smith B A *et al* 1981 *Science* **212** 163–91
[2] Smith B A *et al* 1982 *Science* **215** 504–37
[3] Showalter M R 1997 *Bull. Am. Astron. Soc., 29th DPS Meeting (17 April)*
[4] Showalter M R, Pollack J B, Ockert M E, Doyle L R and Dalton J B 1992 *Icarus* **100** 394–411
[5] Bosh A S, Olkin C B, French R G and Nicholson P D 2002 *Icarus* **157** 57–75
[6] Grün E, Morfill G E and Mendis D A 1984 *Planetary Rings* ed R Greenberg and A Brahic (Tucson, AZ: University of Arizona Press) pp 275–332
[7] Mendis D A, Houpis H L F and Hill J R 1982 *J. Geophys. Res.* **87** 3449–55
[8] Matthews L S, Hyde T W and Barge L B 2003 *J. Geophys. Res.* submitted
[9] Richardson D C 1993 *Mon. Not. R. Astron. Soc.* **261** 396–414
[10] Richardson D C 1994 *Mon. Not. R. Astorn. Soc.* **269** 493–511
[11] Richardson D C 1995 *Icarus* **115** 320–35
[12] Matthews L S 1998 *PhD Thesis* Baylor University Press
[13] Vasut J A and Hyde T W 2001 *IEEE Trans. Plasma Sci.* **29** 231–7
[14] Qiao K and Hyde T W 2003 *J. Phys. A: Math. Gen.* **36** 6109–15
[15] Swint G S, Hyde T W and Matthews L S 2002 *Adv. Space Res.* **29** 1311–4
[16] Wisdom J and Tremaine S 1988 *Astron. J.* **95** 925–40

[17] Barnes J and Hut P 1986 *Nature* **324** 446–8
[18] McGhee C A, Nicholson P D, French R G and Hall K J 2001 *Icarus* **152** 282–315
[19] Showalter J R and Burns J A 1982 *Icarus* **52** 526–44
[20] Connerney J E P 1993 *J. Geophys. Res* **98** 18659–79
[21] Mendis D A and Rosenberg M 1996 *Annu. Rev. Astron. Astrophys.* **32** 419–63
[22] Bringol-Barge L and Hyde T W 2002 *Adv. Space Res.* **29** 1289–94
[23] Juhasz A and Horanyi M 1997 *J. Geophys. Res.* **102** 7237–46
[24] Schaffer L and Burns J A 1994 *J. Geophys. Res.* **99** 17211–23